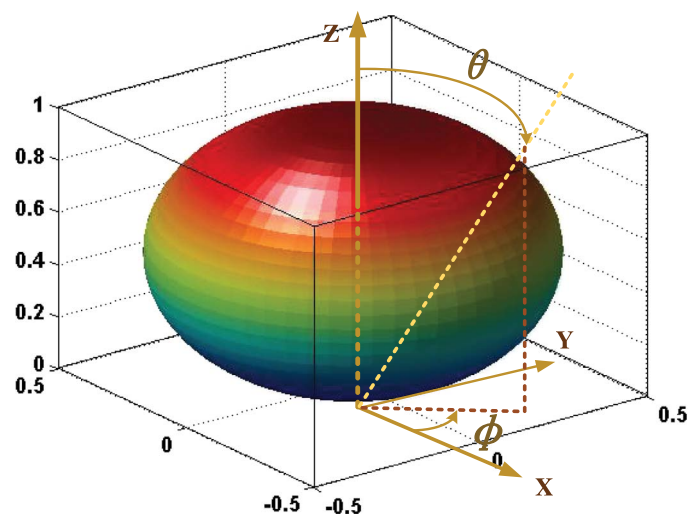# Indoor Optical Wireless Channel Characteristics With Distinct Source Radiation Patterns

Volume 8, Number 1, February 2016

Jupeng Ding
Chih-Lin I, Senior Member, IEEE
Zhengyuan Xu, Senior Member, IEEE

Indoor Optical Wireless Channel Characteristics With Distinct Source Radiation Patterns

Jupeng Ding,[1] **Chih-Lin I,**[2] *Senior Member, IEEE*, **and Zhengyuan Xu,**[1] *Senior Member, IEEE*

[1]Key Laboratory of Wireless-Optical Communications, Chinese Academy of Sciences, School of Information Science and Technology, University of Science and Technology of China, Hefei 230027, China
[2]Green Communication Research Center, China Mobile Research Institute, Beijing 100053, China

Abstract: In conventional indoor optical wireless communication, the transmitter is usually empirically viewed as a source with a Lambertian radiation pattern. This paper comprehensively studies the impact of practical source radiation patterns on channel characteristics, including light-emitting diodes (LEDs) from Nichia and Lumileds Philips. Compared with the Lambertian pattern, differences in impulse and frequency responses, spatial distributions of optical path loss (OPL), and root mean square (RMS) delay spread based on different patterns are clearly observed from simulation. The standard deviation reduction of OPL and RMS delay spread can be up to more than 3.1 dB and 0.138 ns for two practical sources, whereas the respective dynamic ranges of the conventional Lambertian pattern are just 5.1 dB and 0.67 ns. Meanwhile, the radiation pattern from Lumileds Philips provides almost uniform transmission characteristics that are independent of the receiver position.

Index Terms: Optical radiation pattern, path loss, impulse response, root mean square (RMS) delay spread.

1. Introduction

Wireless local area networks (WLANs) and wireless personal area networks (WPANs) have become indispensable and integral parts of our everyday lives, either in a home environment or at public places like hotels, restaurants, and office buildings. Apart from any service requirements, the demand for higher transmission rates is ever increasing, but the established systems will soon reach the capacity limits. Near infrared and visible light based optical wireless communications (OWC) are attractive transmission solutions for WLAN [1]–[6].

In order to evaluate the channel characteristic of OWC, comprehensive models are required. Up to now, OWC channels based on practical light sources are inadequately studied. In radiometry, radiation pattern is adopted to describe the relative light intensity in any direction from the light source. In conventional infrared light based OWC, it is often assumed to emit a Lambertian
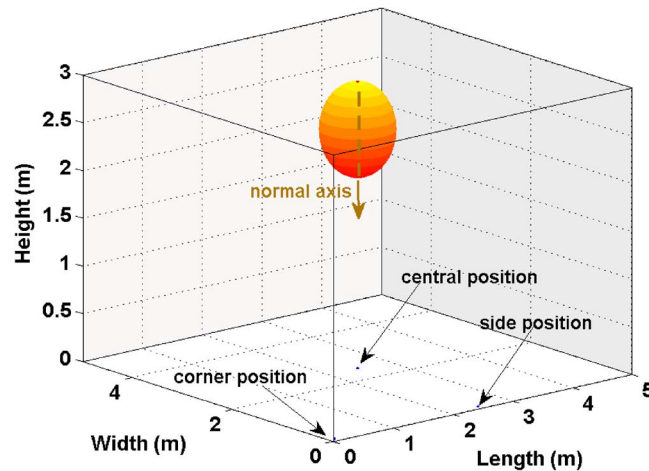
Fig. 1. Indoor scenario with one Lambertian source and three receiver positions.

pattern [1]–[3], [7]–[11]. This assumption is approximately valid in some particular circumstances. For instance, the transmitter uses a cluster of laser diodes (LDs) whose output is passed through a translucent plastic diffuser [12], [13]. A typical indoor scenario with one Lambertian source fixed on the ceiling is shown in Fig. 1. This transmitter configuration cannot describe all cases of visible light based OWC, utilizing white light-emitting diode (LED)-based illumination infrastructure [7]–[9], [14]–[16]. As a matter of fact, both reported measurement work and datasheets from manufacturers show that the radiation patterns of LEDs span a wide range [17].

In fact, these radiation patterns provide a novel freedom to optimize the OWC system performance. Moreover, availability of diverse radiation patterns facilitates system designers to choose the right set of LED patterns according to a range of the pattern-dependent channel descriptions. By replacing the conventional pattern by the selected pattern with better inherent characteristics against multipath dispersion, the link quality and LED coverage can be improved. Meanwhile, packet overhead traditionally adopted to eliminate multipath induced inter-symbol interference (ISI) can be significantly reduced. However, to the best of our knowledge, the OWC channel characteristics under various radiation patterns have not been investigated. In this paper, channel characteristics are compared among one Lambertian source and two typical commercial LEDs, NSPW345CS from Nichia, and LUXEON Rebel from Lumileds Philips, respectively [17]. In particular, impulse response, optical path loss (OPL), root mean square (RMS) delay spread, and transmission bandwidth under different radiation patterns are analyzed. Although we are unable to cover all possible radiation patterns of various commercial LEDs, the channel characteristic dependence to typical radiation patterns are sufficiently revealed for the first time. Numerically, the standard deviation reduction of OPL and RMS delay spread can be up to more than 3.1 dB and 0.138 ns for two practical LED sources, while the respective dynamic ranges of the conventional Lambertian pattern are just 5.1 dB and 0.67 ns. It is noteworthy that the radiation pattern from Lumileds Philips LEDs provides almost uniform transmission characteristics independent of the receiver position. The remainder of this paper is organized as follows. In Section 2, source radiation patterns for three cases are presented. In Section 3, channel characteristics with and without transmitter simplification are compared. The conclusion is given in Section 4.

2. Source Radiation Pattern

The foundation for indoor OWC is based upon understanding of radiation of the source as well as propagation of multiple optical paths between the source and the receiver. Specifically, radiation pattern of a source refers to the spatial intensity distribution of light emanating from the source. Radiant intensity is a measure of radiometric power per unit solid angle, expressed in

watts per steradian. Note that steradian is a dimensionless quantity. This intensity is one key radiometric quantity to characterize the optical property of electromagnetic radiation, which can be expressed as

$$I = \frac{d\Phi}{d\Omega} \tag{1}$$

where $d\Phi$ is the total radiation flux in certain direction, and $d\Omega$ is the corresponding solid angle [18]. Generally, radiant flux Φ is a measure of radiometric power from the source. This received intensity is the ratio of the flux Φ_d collected by the detector aperture over respective solid angle Ω_d subtended by the detector on the source center, i.e. $I = \Phi_d/\Omega_d$. Typically, the angular intensity distribution is measured by holding the source stationary and moving a detector on a hemisphere centered in the source.

Commercial LED sources follow many different radiation patterns, which make it difficult to find a general model for a practical LED array source. Light is produced by spontaneous emission from the light-emitting region of the chip. The final light pattern generated by one LED is the result of the sum of three terms: the light internally reflected inside the lens, the light directly refracted by the encapsulating lens, and the light reflected by the reflecting cup. These contributions generally are continuous functions of the geometry of both reflective cup and the encapsulating lens. In other words, the radiation pattern emitted by the chip is modified by the internal reflection inside the encapsulating lens, the reflection in the back mirror, and the refraction through lens.

To quantify the influence arising from radiation pattern and factors that can effectively dominate the channel merits, it is essential to precisely model distinct source radiation patterns and sufficiently understand the competence of typical pattern of commercial LEDs against multipath effect. The following part of this section focuses on the mathematical characterization and comparative study between conventional Lambertian radiation pattern and two non-Lambertian patterns of LED products from different manufacturers.

2.1. Lambertian Radiation Pattern

In conventional OWC modeling, the angular output power of an optical source is typically modeled by a generalized Lambertian pattern having uniaxial symmetry. This means its intensity is proportional to the viewing angle

$$I(\theta) = \frac{(m+1)}{2\pi}\cos^m\theta \tag{2}$$

where $I(\theta)$ is radiant intensity in units of Candelas, and θ is the spherical polar angle off normal axis (degrees). The index m is related to $\theta_{1/2}$, the source semiangle at half intensity, by $m = \ln(2)/\ln(\cos\phi_{1/2})$ [8]–[10], [12], [13]. In [13], [17], it has been shown that Lambertian sources have the broadest angular characteristics compared with any other sources. In fact, the radiant intensity distribution from a Lambertian source has a circular profile when plotted in polar coordinates. The 3D and 2D radiation patterns of a generalized Lambertian source is shown in Fig. 2(a) and (b), respectively.

In an indoor environment, the optical signals emitted by an abstract source arrive at the receiver via the line of sight (LOS) path or the reflection path from indoor walls, ceiling and floor. In time domain, the impulse response of the channel is adopted to characterize the OWC channel. If a LOS path exists, the impulse response due to this path between the optical source S and the optical receiver R can be given by [13], [16]

$$h^{(0)}(t; S, R) = \begin{cases} \frac{1}{d_0^2} A_R I(\theta)\cos\psi_0\delta\left(t - \frac{d_0}{c}\right), & 0 \leq \psi_0 \leq \text{FOV} \\ 0, & \psi_0 \geq \text{FOV} \end{cases} \tag{3}$$

where A_R is the effective receiver area, d_0 is the direct distance from source S to receiver R, and ψ_0 is the angle of incidence on the receiver location. FOV is the field of view of the receiver, and c is the speed of light.
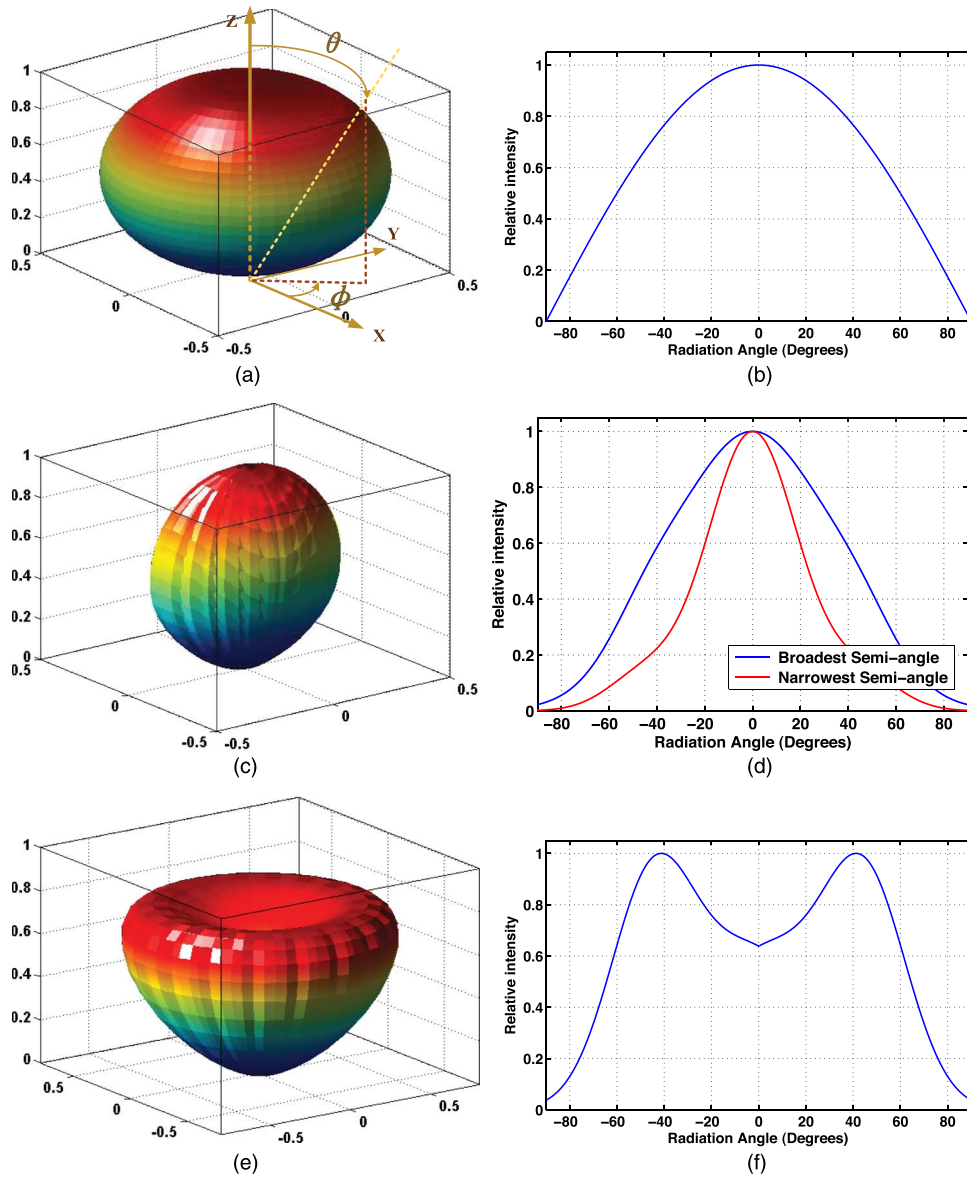
Fig. 2. Three-dimensional radiation pattern of (a) Lambertian m = 1, (c) NSPW345CS from Nichia, (e) LUXEON Rebel from Lumileds Philips; respective 2-D radiation pattern is illustrated in (b), (d), and (f).

Most reflections of indoor environment tend to be diffuse in nature, hence a Lambertian model can be used. Specifically, the time dispersion is imposed by the multipath propagation induced by the interaction between the emitted optical signal and the illuminated walls in an indoor scenario. As the modeling algorithm is finally implemented by computer, the indoor surface must be divided into reflective elements of equal size and the central position is viewed as the the coordinates of the respective reflective element. For the first order reflection, the mentioned interaction can be decomposed into two steps. In the first step, the reflective element is viewed as the abstract receiver and the optical signal reaches the element via LOS path. The impulse response at any lth element ε_l can be given by

$$h^{(0)}(t; S, \varepsilon_l) = \begin{cases} \frac{1}{d_{l,1}^2} A_\varepsilon I(\theta_1) \cos\psi_1 \delta\left(t - \frac{d_{l,1}}{c}\right), & 0 \leq \psi_1 \leq 90° \\ 0, & \psi_1 \geq 90° \end{cases} \tag{4}$$

where A_ε is the area of one reflective element. The distance between a source and this reflective element is represented by $d_{l,1}$, while θ_1 is the irradiance angle of the optical signal and ψ_1 is the incidence angle with respect to the perpendicular direction of the surface, which contains this reflective element. Unlike the case in (3), the FOV of all reflective elements is naturally 90° since all elements are omni-directional in capturing light signal from all incident directions. In the second step, the reflective element absorbs part of captured optical signal power and simultaneously serves as the secondary source to emit the left power. Since the reflective element can be viewed as generalized Lambertian source, i.e. $m = 1$, the final impulse response contribution via this 1st bounce path can be given by

$$h^{(1)}(t; S, \varepsilon_l, R) = \begin{cases} h^{(0)}(t; S, \varepsilon_l) \otimes \rho_l \frac{1}{\pi d_{l,2}^2} A_R \cos\theta_2 \cos\psi_2 \delta\left(t - \frac{d_{l,2}}{c}\right), & 0 \le \psi_2 \le \text{FOV} \\ 0, & \psi_2 \ge \text{FOV} \end{cases} \tag{5}$$

where ρ_l is the reflectivity of the surface to which the reflective element ε_l belongs, $\otimes$ stands for convolution, and $d_{l,2}$ is the distance between the reflective element ε_l and the receiver R, while θ_2 is the irradiance angle of the reflected optical signal, and ψ_2 is the incidence angle with respect to the normal direction of the receiver R.

To obtain the diffuse channel impulse response, the room surface is decomposed into a number of reflecting elements. The existence of multiple propagation paths from these elements does lead to temporal dispersion. The response of the optical impulse undergoing k ($k > 0$) bounce reflections can be calculated recursively [10]

$$h^{(k)}(t; S, R) = \sum_{l=1}^{N} h^{(0)}(t; S, \varepsilon_l) \otimes \rho_l h^{(k-1)}(t; \varepsilon_l, R) \tag{6}$$

where the symbol $\otimes$ denotes convolution, ε_l is the lth reflective element, and N is the number of reflective elements. The specific expression of $h^{(0)}(t; S, \varepsilon_l)$ has been presented in equation (4).

The total impulse response is a sum of the impulse responses from LOS path and reflected paths

$$h(t; S, R) = \sum_{k=0}^{K} h^{(k)}(t; S, R) \tag{7}$$

where K is the upper limit of reflection order. Following work of [7], [10], [11], and [13], up to three order reflections ($K = 3$) are considered.

2.2. NSPW345CS Radiation Pattern

As stated in the above subsection, the Lambertian radiation pattern is presented in one dimensional equation since this pattern is rotationally symmetric in the far field. It will not be applicable if some rotational asymmetries appear in radiation pattern due to emission non-homogeneities on the chip surface and some packaging obstructions [17]. In such a situation, the radiation pattern can show obvious variation in two perpendicular azimuthal directions mainly caused by rotationally asymmetric packaging. For instance, from major manufacturer Nichia, NSPW345CS is one typical LED of such asymmetric radiation pattern. The 3-D description of this elliptic radiation pattern is presented in Fig. 2(c). For clearly illustrating the asymmetry, the 2-D spatial intensity distribution of two azimuthal directions with observable maximum difference is shown in Fig. 2(d). The blue line stands for the cross section with the broadest semi-angle while the red line stands for the perpendicular cross section with the narrowest semi-angle.

Based on the work of [17], this radiation pattern can be expressed as

$$I(\theta, \phi) = \sum_i g1_i \exp\left[-\ln2(|\theta| - g2_i)^2 \left(\frac{\cos^2\phi}{(g3_i)^2} + \frac{\sin^2\phi}{(g4_i)^2}\right)\right] \tag{8}$$

where $g1_1 = 0.13$, $g2_1 = 45°$, $g3_1 = g4_1 = 18°$, $g1_2 = 1$, $g2_2 = 0$, $g3_2 = 38°$, $g4_2 = 22°$, and ϕ is the azimuth angle off the initial direction within the plane that is parallel to the emitting surface of LED.

Generally speaking, to estimate the accuracy of modeled radiation pattern of practical LEDs, the difference between experimental data and modeled equation is usually quantified through the root mean square (RMS) error and the normalized cross correlation (NCC) [17]. The modeled pattern must own high enough accuracy, whatever the type of LED. The RMS error must be less than the standard limit of 5%. Using NCC, the similarity between the simulated pattern and the measured pattern can be demonstrated. For many applications, it is commonly agreed that NCC higher than 99% is capable to provide sufficient accuracy. According to [17], the NCC of this radiation pattern modeling of NSPW345CS is 99.97% while the related RMS error is 1.01%, which can satisfy the accuracy requirement.

By replacing $I(\theta)$ to $I(\theta, \phi)$ of equation (8), the LOS impulse response expression of equation (3) and (4) for NSPW345CS Radiation Pattern can be obtained. By following the customized LOS impulse responses, the expressions of (5) to (7) for non-LOS, and finally, total impulse response can be renewed accordingly.

2.3. LUXEON Rebel Radiation Pattern

Similar to antennas in radio frequency, LED also exhibits directive nature, which means the radiation intensity is not uniform in all directions. The property of radiating more strongly in some directions than in others is called the directivity of the source. For discussed Lambertian and NSPW345CS radiation pattern, the maximum intensity still appears in the normal direction of LED. However, such directivity mode is not consistent with all LEDs. Typically, the maximum intensity of Lower Bound LUXEON Rebel from Lumileds Philips appears in all directions with certain angle off the normal axis. In Fig. 2(e) and (f), the 3-D and 2-D radiation pattern of LUXEON Rebel is given, which is of loose circular cone shape, but partial hollow. This maximum intensity appears in the direction of about 45° off the normal axis.

Inherited from [17], this angular distribution of this non-Lambertian pattern can be characterized as

$$I(\theta) = \sum_i g1_i \exp\left[-\ln 2 \left(\frac{|\theta| - g2_i}{g3_i} \right)^2 \right] \tag{9}$$

where $g1_1 = 0.76$, $g2_1 = 0°$, $g3_1 = 29°$, $g1_2 = 1.10$, $g2_2 = 45°$, and $g3_2 = 21°$. Similar to the case of NSPW345CS, the com-pact analytical representation of this pattern is a sum of modified Gaussian functions as well. Nevertheless, unlike the previous case, the intensity is independent of the azimuthal angle that basically dominates its symmetry.

Similar to the mentioned case of NSPW345CS Radiation Pattern, the respective expression of $I(\theta)$ must be replaced by (9) in (3) and (4) to obtain the needed LOS impulse responses for LUXEON Rebel Radiation Pattern. Based on these characterized LOS responses, the response of each bounce reflection and the whole impulse response for this radiation pattern can be easily obtained following (5) to (7), respectively.

3. Numerical Results and Discussion

To investigate the effect of distinct radiation pattern on OWC channel characteristics, a typical indoor scenario of 5 m × 5 m × 3 m is introduced, which is consistent with the setting of [13], as shown in Fig. 1. Only one LED source is fixed at the center of the ceiling. The normal of the source is vertically downwards. In the spatial resolution of indoor surface, following the work of [7], [10], [11], one meter is uniformly divided into 20 parts, eight parts, and four parts for the first, second, and third reflections, respectively. At the same time, the reflectance for the ceiling is 0.8 while the counterparts for the surrounding walls and the floor are 0.8 and 0.3, accordingly. Additionally, for convenience of comparison of published classic work with conventional source

TABLE 1

Parameters for transmission characteristics simulation

Parameters	Value
Room size	5 m $\times$ 5 m $\times$ 3 m
Reflectance of ceiling	0.8
Reflectance of wall	0.8
Reflectance of floor	0.3
Impulse response time resolution	0.2 ns
Reflective element size for 1st reflection	5 cm $\times$ 5 cm
Reflective element size for 2nd reflection	12.5 cm $\times$ 12.5 cm
Reflective element size for 3rd reflection	25 cm $\times$ 25 cm
Coordinates of LED source	(2.5, 2.5, 3.0) m
Elevation of LED source	-90 deg.
Azimuth of LED source	0 deg.
Height of LED source	3 m
Detection physical area of receiver	1 cm^2
FOV of receiver	85 deg.
Elevation of receiver	90 deg.
Azimuth of receiver	0 deg.
Height of receiver	0 m
Spacing of neighbouring receiver positions	0.2 m
Amount of all concerned receiver positions	625 (25$\times$25)
Coordinates of central receiver position	(2.5, 2.5, 0.0) m
Coordinates of side receiver position	(2.5, 0.1, 0.0) m
Coordinates of corner receiver position	(0.1, 0.1, 0.0) m

radiation pattern [7], [8], [13], the receiver with 85° field of view is placed on the floor. Table 1 shows the main parameters for transmission characteristics simulation.

In the following subsections, the quantified multipath channel performances of cases with three distinct radiation patterns are specifically evaluated in terms of impulse response, frequency response, RMS delay spread, and OPL.

3.1. Impulse and Frequency Response

As mentioned earlier, the temporal spreading engendered by multipath propagation can be described by the channel impulse response $h(t)$, which characterizes the channel in the time domain. On the other hand, the frequency response $H(f)$ characterizes the channel as a function of frequency

$$H(f) = \int_{-\infty}^{\infty} h(t)e^{-j2\pi ft}dt \qquad (10)$$

that is the Fourier transform of the channel impulse response $h(t)$. Note that the frequency response of the dispersive OWC channel exhibits a low pass characteristic in the electrical domain. Naturally, the OWC channel's achievable transmission bandwidth constitutes an important metric of the transmission potential. In practice, the 3-dB channel transmission bandwidth $f_{-3\ dB}$ is expressed as

$$|H(f_{-3\ dB})|^2 = 0.5|H(0)|^2. \qquad (11)$$

Usually, the 3-dB transmission bandwidth is analyzed at typical receiver locations. Due to the symmetry of the described indoor geographical setting, the impulse responses of three key receiver positions are evaluated. Specifically, the three positions are located in the center, the side, and the corner of the floor, as shown in Fig. 1. The coordinates are (2.5, 2.5, 0) m, (2.5, 0.1, 0) m, and (0.1, 0.1, 0) m, respectively. Obviously, a right triangle is surrounded by the three positions. Thanks to the symmetry to the room center, the whole floor can be composed by eight right triangle area of equal size. Therefore, one right triangle area can represent all channel characteristics of the
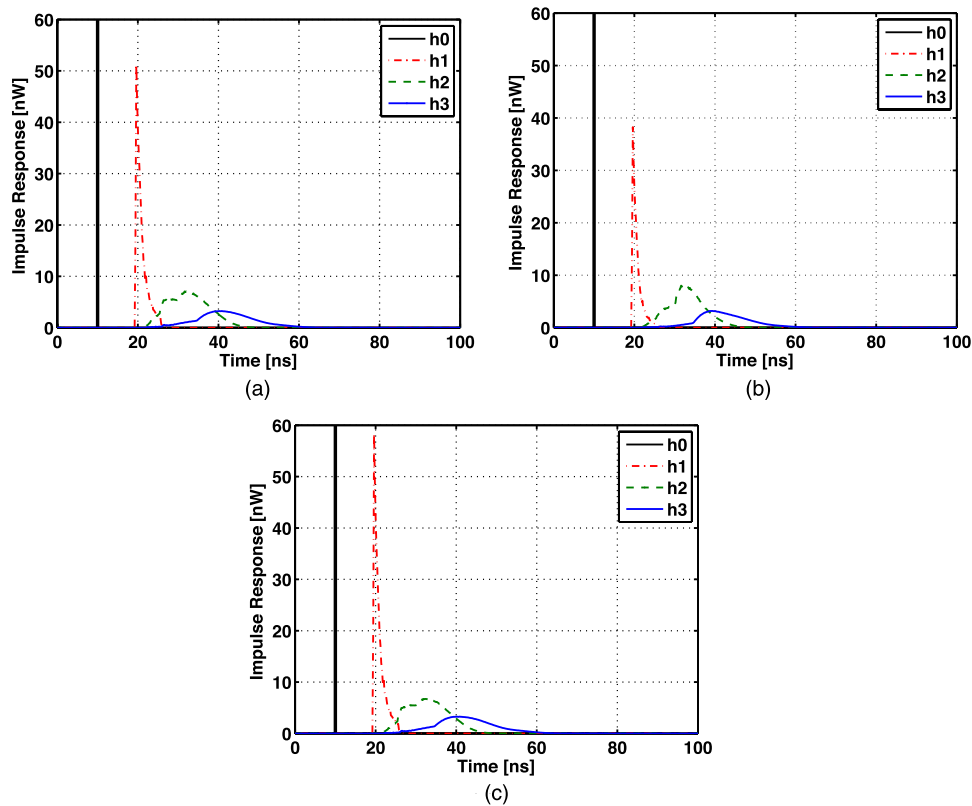
Fig. 3. Impulse response of corner position for (a) Lambertian, (b) NSPW345CS, and (c) LUXEON radiation pattern.

whole receiver plane. In the mean time, the channel characteristic of any position within this triangle can be viewed as a transition among the counterparts of three mentioned key positions. Independent of specific position, any channel impulse response can be expressed by a discrete low pass impulse response. In the central position, the LOS components from three radiation patterns still appear with 10 ns propagation delay, as seen in Fig. 3. For all three patterns, the time interval between the LOS part and the beginning of diffuse reflection parts is about 10 ns.

Since this central position is just below the source on the ceiling, the LOS contribution dominates the channel characteristic to the maximum extent. One useful ratio of received impulse power via certain order reflection paths to the total received impulse power is involved in the following analysis. Viewing the case of Lambertian radiation pattern, the ratio of first, second and third reflections is limited within 9.0%, 9.8%, and 5.7%, respectively. As for the case of NSPW345CS radiation pattern, the respective ratio can be further reduced to 3.0%, 4.7%, and 2.6% because more emitted power is concentrated in the normal direction of the source. For the third radiation pattern, the related three ratios in collected impulse power are just 14.1%, 14.2%, and 8.6%, as given in Table 2. The reason of this phenomenon is that the maximum radiation intensity does not appear along the normal direction any more.

Fig. 4(a) shows the channel magnitude responses of the central position, which can be obtained from the discrete Fourier transform of the above channel impulse responses [10]. The DC gains of both NSPW345CS and LUXEON Rebel radiation patterns are close to −101.3 dB and −109.9 dB while the counterpart of Lambertian pattern is more than −106.6 dB that is mainly elevated by the various other reflection components. Generally, the baseband −3 dB channel bandwidth is usually adopted to quantify the low pass characteristic, which corresponds to the minimum frequency where the magnitude of the transfer function is 3 dB below its maximum value, i.e., DC gain [10]. At the central position, for the Lambertian and NSPW345CS

TABLE 2

Comparison of impulse response components ratio

|		Percentage of the quantity of interest to the whole impulse response (%)			
	Radiation Pattern	LOS	1st Reflection	2nd Reflection	3rd Reflection
Central Position	Lambertian	75.5	9.0	9.8	5.7
	NSPW345CS	89.7	3.0	4.7	2.6
	LUXEON®Rebel	63.1	14.1	14.2	8.6
Side Position	Lambertian	50.2	22.2	17.5	10.1
	NSPW345CS	47.5	19.5	21.1	11.9
	NSPW345CS side 2	61	20.3	12.3	6.4
	LUXEON®Rebel	51.2	23.1	16.2	9.5
Corner Position	Lambertian	36.6	21.4	22.6	19.4
	NSPW345CS	36.7	19.3	23.5	20.5
	LUXEON®Rebel	38.9	21.9	21.2	18.0
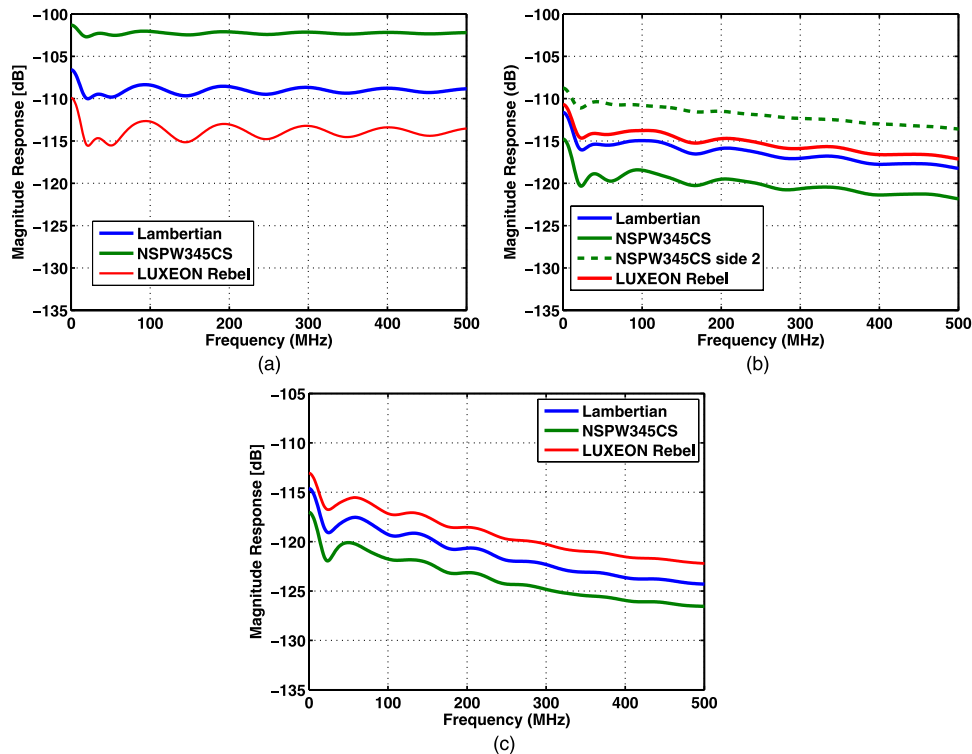
Fig. 4. Channel frequency response characteristics under three radiation patterns at (a) central position, (b) side position, and (c) corner position.

radiation patterns, as the receiver can always capture sufficient LOS contribution that dominates the final channel frequency characteristic, the −3 dB channel bandwidth is almost ideal. However, for the last pattern, the respective −3 dB channel bandwidth is just 12.2 MHz due to remarkable channel temporal dispersion. In this subsection, all concerned −3 dB channel bandwidths are summarized in Table 3.

At the side position, for all radiation patterns, the time interval between the LOS components and the beginning of diffuse components no longer exist because the direct distance between the source and the receiver is increased to more than 3.8 m from the original 3 m, which is almost equal to the shortest diffuse reflection path. Similar to the case of the central position,

TABLE 3

Comparison of −3-dB channel bandwidths

	-3 dB channel bandwidth (MHz)		
	Central Position	Side Position	Corner Position
Lambertian	ideal	14.6	15.9
NSPW345CS	ideal	13.4 or 225.8	14.6
LUXEON®Rebel	12.2	15.9	17.1

the Lambertian radiation pattern unavoidably captures considerable reflection components from the surrounding wall surfaces. Since this pattern just slowly decays the intensity in directions facing the reflective surfaces, the respective ratio of LOS contribution is reduced to 50.2% while the ratio of first, second and third reflections is increased up to impressing 22.2%, 17.5%, and 10.1%, respectively. For clarity, the deteriorative time dispersion is mapped onto the frequency domain, as given in Fig. 4(b). Unlike the LOS contribution, the significant impact from the diffuse reflection, especially the high order reflection, concentrates in the low frequencies. Therefore, although the DC gain can still be kept at −111.6 dB from original −106.6 dB, the −3 dB channel bandwidth decreases to only 14.6 MHz from the ideal case. As for the asymmetric ellipsoid radiation pattern of NSPW345CS, there are two different kinds of side positions facing semi-major axis and semi-minor axis of ellipsoid, respectively. Therefore, apart from the mentioned side position, another side position near to the same corner, i.e. (0.1, 2.5, 0) labeled NSPW345CS side 2 must be observed for this pattern to get the sufficient knowledge of the multipath channel characteristic. Actually, for the side position of (2.5, 0.1, 0), the ratio of first, second and third reflection is up to 19.5%, 21.1%, and 11.9%. However, the diffuse reflection influence to the position of (0.1, 2.5, 0), i.e. NSPW345CS side 2 position, is lightly alleviated with the respective three ratios of 20.3%, 12.3% and 6.4%. In Fig. 4(b), the channel characteristic discrepancy between the two side positions is apparently illustrated. For the side position of (2.5, 0.1, 0), the −3 dB channel bandwidth is just about 13.4 MHz while the counterpart of the other side position is 225.8 MHz that means that, at the latter side position, the NSPW345CS pattern can resist the affect induced by multipath dispersion. In the same side position, the LOS ratio is maintained up to 51.2% that is close to the ratio of 63.1% of the central position. In frequency domain, although the magnitude level is reduced to −110.7 dB, the −3 dB channel bandwidth is just about 15.9 MHz due to the absence of dominant LOS contribution in channel characteristic.

Generally, the most severe channel condition occurs when the receiver is located at the corner position since the optical signal has to undergo the longest propagation path to reach this position. For the Lambertian radiation pattern, the components of the LOS and the multiple diffuse reflections almost start to appear at 15 ns simultaneously. Correspondingly, the ratio of LOS is ultimately decreased to no more than 36.6% while the ratio of first, second and third reflections is up to 21.4%, 22.6% and 19.4%, respectively. Once this impulse response is mapped onto the frequency domain, the baseband transmission bandwidth is further reduced to 15.9 MHz with just −114.6 dB DC gain, as seen in Fig. 4(c). Similarly, for the NSPW345CS radiation pattern, the LOS ratio is finally reduced to 36.8% that is unable to dominate the channel characteristic. The respective frequency response curve is presented in Fig. 4(c), while the transmission bandwidth is kept at 14.6 MHz level. For the third radiation pattern, as the LOS part totally connects with the temporal response tail caused by multipath reflection, the absolute response from multiple reflections is still quite significant. Consequently, the specific ratio of first, second and third reflections is just 21.9%, 21.2%, and 18.0%. Regarding frequency response, apart from the reduced DC gain of −113.1dB, the −3 dB channel bandwidth is 17.1 MHz, which is distinctly dependent on the receiver position.

Above numerical results of time or frequency response demonstrate that if the actual radiation pattern, such as NSPW345CS case, can be designed to be directed at distant receiver postion,
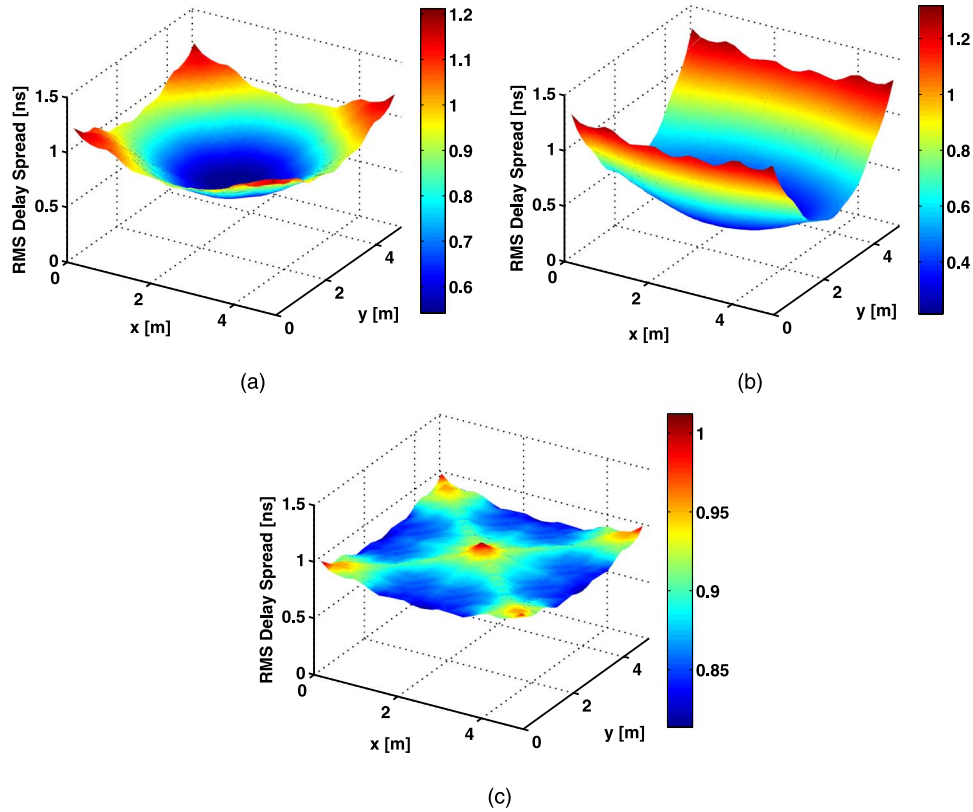
(a)

(b)

(c)

Fig. 5. RMS delay spread distribution of (a) Lambertian m = 1, (b) NSPW345CS from Nichia, and (c) LUXEON Rebel from Lumileds Philips.

such as side 2 position, the channel condition can be dramatically improved. In the meantime, once all maximum radiation direction deviates the normal direction of source as the LUXEON Rebel case, the transmission condition of conventional best position, which is just under the source, will degrade to a power level below the ordinary level.

3.2. Root Mean Square (RMS) Delay Spread

The multipath dispersion can cause inter-symbol interference (ISI) in the received signal. And ISI can be measured by the RMS delay spread. Therefore, the performance of an OWC system is quite sensitive to the RMS delay spread [7], [10], [11], [13]. If the total delay spread of the collected signal is smaller than the symbol duration and the system does not use techniques to mitigate the dispersion, then the bit error rate performance significantly degrades [13].

In order to numerically compare the temporal dispersion of different channels, the RMS delay of the collected signal is evaluated from the simulated channel impulse response. The RMS delay D of the collected signal may be expressed from the channel impulse response by

$$D = \left[\frac{\int (t-\mu)^2 h^2(t)\,dt}{\int h^2(t)\,dt} \right]^{\frac{1}{2}} \tag{12}$$

where the mean excess delay μ can be computed from the following expression:

$$\mu = \frac{\int t h^2(t)\,dt}{\int h^2(t)\,dt} \tag{13}$$

TABLE 4

Comparison of RMS delay-spread statistics

RMS delay-spread (ns)			
Radiation Pattern	Dynamic Range	Average	Std deviation
Lambertian	0.54~1.21	0.83	0.17
NSPW345CS	0.21~1.32	0.66	0.32
LUXEON®Rebel	0.81~1.01	0.88	0.032

and the limits of integration in (7) and (8) extend over all time [13]. It should be emphasized that since $h(t)$ is fixed for a given configuration, as is the RMS delay spread. Thus, optical paths with relatively strong power and simultaneously long delays contribute significantly to the delay spread. For the case of the Lambertian source, the resulting RMS delay spread profile is symmetric with circular sink in the central area that is just under the position of source, as shown in Fig. 5(a). The dynamic range of the delay spread over the coverage plane is 0.67 ns (maximum, average and minimum simulated delay spreads are 1.21 ns, 0.83 ns and 0.54 ns, respectively). The results of two practical LEDs are totally different. As shown in Fig. 2(c) and (d), the radiation pattern of NSPW345CS from Nichia is not isotropic any more. Accordingly, the distribution of RMS delay spread is no longer symmetric since two opposite wall surfaces can capture much less LOS signal than the left two surfaces, as presented in Fig. 5(b). Under this radiation pattern setting, the maximum, average and minimum values within the test scenario are 1.32 ns, 0.66 ns and 0.21 ns, respectively, which results in a dynamic range of about 1.11 ns. Moreover, the central sink is no longer circular, but oval in shape.

More attention should be paid to the channel characteristics of LUXEON Rebel from Lumileds Philips. Compared with the above two cases, slight increase of RMS delay spread is achieved with average value of 0.88 ns. Despite its isotropic radiation pattern, the maximum does not appear at the normal direction but in certain departure angles to this direction. In this situation, for the central area, the LOS signal does not play a dominant role. For the side and corner areas, the contribution of LOS signal is improved. The minimum of RMS delay spread constitutes an irregular ring area, not a circle area as before. As shown in Fig. 5(c), the dynamic range of delay spread is just 0.2 ns (maximum and minimum delay spreads are 1.01 ns and 0.81 ns, respectively). Table 4 shows the all results of RMS delay spread statistics.

Up to now, orthogonal frequency division multiplexing (OFDM) modulation is viewed as a promising technique in various indoor OWC systems [19]–[21]. The basic concept of OFDM is that the serial high-speed data stream is transmitted in parallel on multiple orthogonal subcarriers. The channel multipath dispersion still remains as harmful factor that may destroy the orthogonality among the subcarriers in an OFDM scheme [19]–[22]. To warrant the performances of OFDM-based systems, there must be some means of dealing with the inter-symbol interference (ISI) over the multipath channel. A guard interval, i.e. cyclic prefix (CP) between two consecutive OFDM symbols is essential, which takes a number of samples from the end of each symbol and copies them as the prefix of the OFDM symbol. Conventional OFDM systems usually choose the length of CP based on the average or even maximum RMS delay spread of the multipath channel [19], [22]. Thus the CP overhead is proportional to the maximum delay spread. Based on above analysis in this subsection, the CP overhead of NSPW345CS radiation pattern is 9.09% larger than the counterpart of the conventional Lambertian radiation pattern. On the other hand, the overhead of LUXEON Rebel radiation pattern is reduced to 83.5% of Lambertian case. The reduction of CP overhead is quite valuable in improving the throughput of OWC systems, especially in the high speed cases. Furthermore, both the dynamic range and the standard deviation of the LUXEON pattern are obviously less than the counterparts of the other two patterns, which means that the function of mentioned CP design is sufficiently utilized once the source pattern is deliberately designed to obey LUXEON pattern.
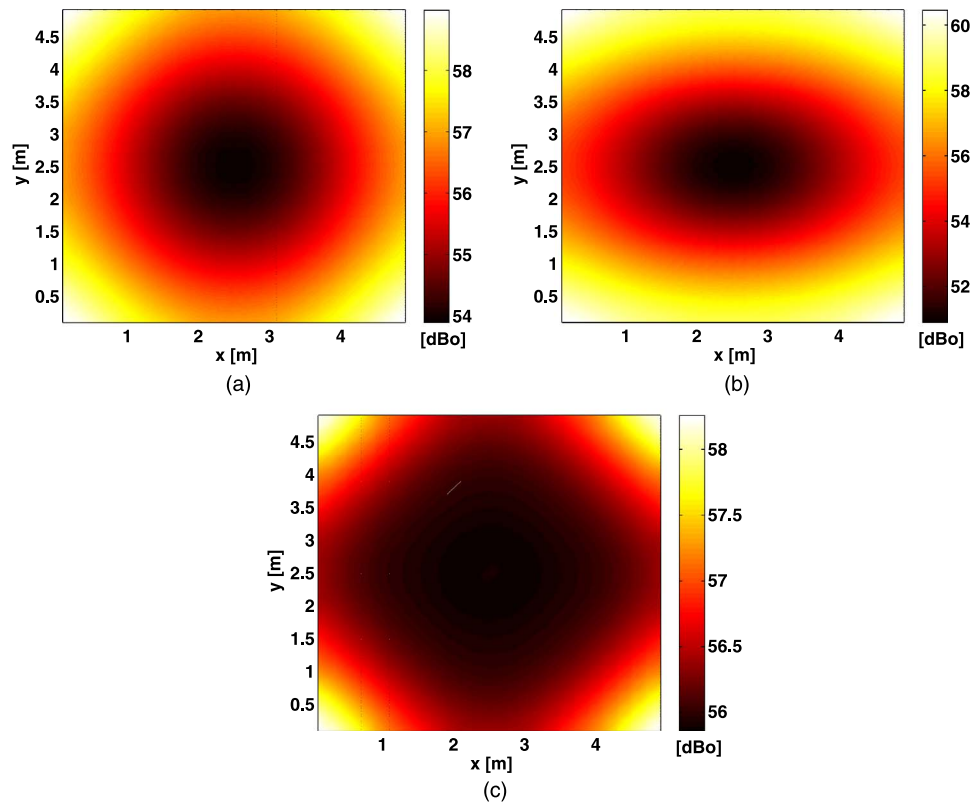
Fig. 6. Optical path loss of (a) Lambertian m = 1, (b) NSPW345CS from Nichia, and (c) LUXEON Rebel from Lumileds Philips.

3.3. Optical Path Loss (OPL)

For OWC, as one of the major impairments, the OPL is usually adopted to evaluate the attenuation of the optical signal due to its reflections and propagation in the free space [12], [13]. When the sensitivity of the detector is given, the required emitting power is mainly dependent on the OPL of channel. For indoor OWC, available transmitter signal power is often limited by considerations of power consumption. This implies that the OWC system should be delicately designed to minimize path loss. The multipath OPL is defined by the logarithm of the DC direct current (DC) value of the channel transfer function and is expressed in optical dB (dBo): $PL = -10\log_{10}H(0)$, where the channel DC gain can be calculated from the impulse response by $H(0) = \int h(t)dt$ [12], [13]. The three different variants of the source radiation patterns specified above are compared from the view of OPL.

The simulated three OPL distribution diagrams on the receiving plane are shown in Fig. 6, the brighter the more OPL. The resulting OPL of the Lambertian radiation pattern can be viewed as a function of receiver position within the typical room. It can be observed that the low OPL is mainly distributed near the center of the receiving plane, and the OPL rises dramatically as the distance to the center increases. This indicates that this radiation pattern emanates mainly onto a moderate circular area of the plane. The minimum and maximum values are 53.9 dBo and 59.0 dBo, respectively, which results in a dynamic range of about 5.1 dBo. For about 80% of the receiving plane, the OPL is less than 57.3 dBo. In the case of NSPW345CS radiation pattern, the dynamic range of the OPL is about 9.6 dBo. The minimum and maximum values are 50.9 dBo and 60.5 dBo. For about 80% of the receiving plane, the OPL is less than 58.3 dBo that mainly lies in the dark domain of oval shape, as shown in Fig. 6(b). By comparing the results of the NSPW345CS and Lambertian radiation pattern, there is an increase of approximately 0.6 dBo in the worst-case OPL.

TABLE 5

Comparison of optical path loss statistics

Optical path loss (dBo)		
Radiation Pattern	Dynamic Range	Average
Lambertian	53.9∼59.0	56.4
NSPW345CS	50.9∼60.5	56.5
LUXEON®Rebel	55.9∼58.3	56.5

The OPL profile of LUXEON Rebel pattern is plotted in Fig. 6(c). The minimum and maximum OPL over the indoor area are 55.9 dBo and 58.3 dBo, respectively, giving a dynamic range of 2.4 dBo that reduces 2.7 dBo from original Lambertian case. This variation means that the LUXEON Rebel pattern illustrates superior uniformity in OPL. Under this condition, the worst channel losses still appear at the boundary of the room, especially in four corners. Thanks to the isotropy of this radiation pattern, OPL steadily increases with the radius to the center. For about 80% of the observed positions, the OPL is less than 56.8 dBo. Table 5 shows the all results of OPL delay spread statistics. Above numerical results jointly show that the third pattern relaxes the need of large power dynamic range of electric components used in transmitter. In the meantime, the better mobility can be provided to receiver since the more uniform coverage performance can be assured by the LUXEON pattern.

4. Conclusion

The effects of distinct source radiation patterns on multipath characteristics of OWC channels have been investigated by deterministic modeling simulation. Compared to the conventional Lambertian pattern and non-isotropic NSPW345CS radiation pattern, the pattern of LUXEON Rebel is demonstrated to be a more effective candidate to mitigate the effects of multipath temporal dispersion for a typical indoor scenario. Under this radiation pattern, the maximum radiant intensity is liberated from traditional normal direction, which jointly improves uniformity of coverage and freedom of mobility. The superiority of LUXEON Rebel pattern lies in the reduced delay spread Std deviation to less than 0.032 ns while the counterpart of other two patterns gives 0.17 ns and 0.32 ns, respectively. In the view of OPL, better uniformity with 2.7 dBo reduction in dynamic range can be realized by this pattern at the price of slight elevation in minimum OPL. Association of channel characteristic with radiation pattern paves a new way to improve mobility and robustness performance of the OWC systems by screening, design, and optimization of source radiation patterns.

References

[1] A. Sevincer, A. Bhattarai, M. Bilgi, M. Yuksel, and N. Pala, "LIGHTNETs: Smart LIGHTing and Mobile Optical Wireless NETworks—A survey," *IEEE Commun. Surveys Tuts.*, vol. 15, no. 4, pp. 1620–1641, 4th Quart. 2013.
[2] I. Din and H. Kim, "Energy-efficient brightness control and data transmission for visible light communication," *IEEE Photon. Technol. Lett.*, vol. 26, no. 8, pp. 781–784, Apr. 2014.
[3] A. Burton, H. L. Minh, Z. Ghassemlooy, E. Bentley, and C. Botella, "Experimental demonstration of 50-Mb/s visible light communications using 4 × 4 MIMO," *IEEE Photon. Technol. Lett.*, vol. 26, no. 9, pp. 945–948, May 2014.
[4] J. Ding, Z. Xu, and L. Hanzo, "Accuracy of the point-source model of a multi-LED array in high-speed visible light communication channel characterization," *IEEE Photon. J.*, vol. 7, no. 4, Aug. 2015, Art. ID 1600714.
[5] I. Ansari, M.-S. Alouini, and J. Cheng, "Ergodic capacity analysis of free-space optical links with nonzero boresight pointing errors," *IEEE Trans. Wireless Commun.*, vol. 14, no. 8, pp. 4248–4264, Aug. 2015.
[6] F. Yang, J. Cheng, and T. Tsiftsis, "Free-space optical communication with nonzero boresight pointing errors," *IEEE Trans. Commun.*, vol. 62, no. 2, pp. 713–725, Feb. 2014.
[7] J. Ding, Z. Huang, and Y. Ji, "Evolutionary algorithm based uniform received power and illumination rendering for indoor visible light communication," *J. Opt. Soc. Amer. A, Opt. Image Sci.*, vol. 29, no. 6, pp. 971–979, May 2012.
[8] J. Grubor, S. Randel, K.-D. Langer, and J. Walewski, "Broadband information broadcasting using LED-based interior lighting," *J. Lightw. Technol.*, vol. 26, no. 24, pp. 3883–3892, Dec. 2008.
[9] J. Ding and Z. Xu, "Performance of indoor VLC and illumination under multiple reflections," in *Proc. 6th Int. Conf. WCSP*, Oct. 2014, pp. 1–6.

[10] J. Ding, K. Wang, and Z. Xu, "Accuracy analysis of different modeling schemes in indoor visible light communications with distributed array sources," in *Proc. 9th Int. Symp. CSNDSP*, Jul. 2014, pp. 1005–1010.

[11] J. Ding, K. Wang, and Z. Xu, "Impact of LED array simplification on indoor visible light communication channel modeling," in *Proc. 9th Int. Symp. CSNDSP*, Jul. 2014, pp. 1159–1164.

[12] S. Jovkova and M. Kavehard, "Multispot diffusing configuration for wireless infrared access," *IEEE Trans. Commun.*, vol. 48, no. 6, pp. 970–978, Jun. 2000.

[13] J. Barry, J. Kahn, W. Krause, E. Lee, and D. Messerschmitt, "Simulation of multipath impulse response for indoor wireless optical channels," *IEEE J. Sel. Areas Commun.*, vol. 11, no. 3, pp. 367–379, Apr. 1993.

[14] J. Gancarz, H. Elgala, and T. Little, "Impact of lighting requirements on VLC systems," *IEEE Commun. Mag.*, vol. 51, no. 12, pp. 34–41, Dec. 2013.

[15] Z. Wang *et al.*, "Performance of dimming control scheme in visible light communication system," *Opt. Exp.*, vol. 20, no. 17, pp. 18861–18868, Aug. 2012.

[16] J. Ding and Y. Ji, "Evolutionary algorithm-based optimisation of the signal-to-noise ratio for indoor visible-light communication utilising white light-emitting diode," *IET Optoelectron.*, vol. 6, no. 6, pp. 307–317, Dec. 2012.

[17] I. Moreno and C.-C. Sun, "Modeling the radiation pattern of LEDs," *Opt. Exp.*, vol. 16, no. 3, pp. 1808–1819, Feb. 2008.

[18] A. Ryer, *Light Measurement Handbook*. Peabody, MA, USA: Int. Light, 1997.

[19] J. Armstrong, "OFDM for optical communications," *J. Lightw. Technol.*, vol. 27, no. 3, pp. 189–204, Feb. 2009.

[20] S. Dissanayake and J. Armstrong, "Comparison of ACO-OFDM, DCO-OFDM and ADO-OFDM in IM/DD systems," *J. Lightw. Technol.*, vol. 31, no. 7, pp. 1063–1072, Apr. 2013.

[21] S. Dimitrov and H. Haas, "Information rate of OFDM-based optical wireless communication systems with nonlinear distortion," *J. Lightw. Technol.*, vol. 31, no. 6, pp. 918–929, Mar. 2013.

[22] Y. Cho, W. Kim, J. Yang, and C. Kang, *MIMO-OFDM Wireless Communications With MATLAB*. Piscataway, NJ, USA: Wiley-IEEE Press, 2010.